Journal of Atmospheric and Solar-Terrestrial Physics 71 (2009) 289–299

Contents lists available at ScienceDirect

Journal of
Atmospheric and Solar-Terrestrial Physics

journal homepage: www.elsevier.com/locate/jastp

The Aeronomy of Ice in the Mesosphere (AIM) mission: Overview and early science results

James M. Russell III[a,*], Scott M. Bailey[b], Larry L. Gordley[c], David W. Rusch[d], Mihály Horányi[d], Mark E. Hervig[c], Gary E. Thomas[d], Cora E. Randall[d], David E. Siskind[e], Michael H. Stevens[e], Michael E. Summers[f], Michael J. Taylor[g], Christoph R. Englert[e], Patrick J. Espy[h], William E. McClintock[d], Aimee W. Merkel[d]

[a] Center for Atmospheric Sciences, Hampton University, 23 Tyler Street, Hampton, VA 23668, USA
[b] Bradley Department of Electrical and Computer Engineering, Virginia Polytechnical Institute and State University, Blacksburg, VA 24061, USA
[c] GATS, Inc., 11864 Cannon Boulevard, Suite 101, Newport News, VA 23606, USA
[d] Laboratory for Atmospheric and Space Physics, 1234 Innovation Drive, Boulder, CO 80303, USA
[e] Space Science Division, Naval Research Laboratory, Washington DC 20375, USA
[f] Department of Physics, George Mason University, Fairfax, VA 22030, USA
[g] Center for Atmospheric and Space Sciences and Physics Department, Utah State University, Logan, UT 84322, USA
[h] Department of Physics, Norwegian University of Science and Technology, Høgskoleringen 5, NO-7491 Trondheim, Norway

ARTICLE INFO

Article history:
Accepted 21 August 2008
Available online 11 September 2008

Keywords:
Polar mesospheric clouds
Mesosphere
Remote sensing
Gases
Particles
Global change

ABSTRACT

The Aeronomy of Ice in the Mesosphere (AIM) mission was launched from Vandenberg Air Force Base in California at 1:26:03 PDT on April 25, 2007 becoming the first satellite mission dedicated to the study of polar mesospheric clouds. A Pegasus XL rocket launched the satellite into a near perfectly circular 600 km sun synchronous orbit. AIM carries three instruments selected because of their ability to provide key measurements needed to address the AIM goal which is to determine why these clouds form and vary. The instrument payload includes a nadir imager, a solar occultation instrument and an in-situ cosmic dust detector. Detailed descriptions of the science, instruments and observation scenario are presented. Early science results from the first northern and southern hemisphere seasons show a highly variable cloud morphology, clouds that are ten times brighter than measured by previous space-based instruments, and complex features that are reminiscent of tropospheric weather phenomena. The observations also confirm a previously theorized but never before directly observed population of small ice particles in the altitude region above the main Polar Mesospheric Cloud (PMC) layer that are widely believed to be the indirect cause of summertime radar echoes.

© 2008 Elsevier Ltd. All rights reserved.

1. Introduction

Polar Mesospheric Clouds (PMCs), as they are called when viewed from satellites, are Earth's highest clouds, occupying the atmospheric region near the high-latitude summer mesopause at ~83 km. They typically extend from ~55° latitude to the geographic pole, occurring in each summer in both hemispheres between about mid-May to mid-August in the North and mid-November to mid-February in the South. The polar upper mesosphere becomes the coldest place on earth around summer solstice, when the temperature plummets below 130 K. Known as noctilucent, or "night-shining" clouds (NLCs) as seen by ground-based observers (Fig. 1), their name derives from the fact that they are seen at evening or morning twilight, when the lower atmosphere is in darkness, but the upper atmosphere is still sunlit. First identified over 120 years ago (Leslie, 1885), their nature as water–ice particles was not confirmed observationally until relatively recently (Hervig et al., 2001). There is great interest in PMCs because they are changing in ways that are not understood. They are occurring more frequently, becoming brighter and seem to be appearing at lower latitudes than ever before (Deland et al., 2006, 2007; Taylor et al., 2002). This behavior suggests a possible connection with global change occurring at lower altitudes.

Due to their sensitivity to changes in the environment, PMCs are expected to respond to long-term global change, and may be a modern phenomenon associated with the rise of greenhouse gases in the industrial era (Thomas et al., 1989a, b) although there is not unanimous opinion in the scientific community on this point (see von Zahn, 2003; Thomas et al., 2003). Recent work based on analysis of data from the solar backscattered ultraviolet (SBUV) series of satellites, reveals that an increase of ~5% per

* Corresponding author. Tel.: +1 757 728 6893; fax: +1 757 727 5090.
E-mail address: james.russell@hamptonu.edu (J.M. Russell III).

1364-6826/$ - see front matter © 2008 Elsevier Ltd. All rights reserved.
doi:10.1016/j.jastp.2008.08.011

Fig. 1. Noctilucent cloud photographed by Tom Eklund, July 28, 2001, Valkeakoski, Finland.

decade in PMC brightness has occurred over the past 27 years (DeLand et al., 2007). Lack of understanding of how PMCs form and why they vary, their possible connection with global change and their striking appearance have stimulated a long-term effort resulting in hundreds of measurements of PMC properties and related parameters (e.g. temperature, turbulence, meteoric dust, and ionization) using sounding rockets (e.g. Walchli et al., 1993; Lübken, 1999; Goldberg et al., 2006) and lidars (see e.g. Hansen et al., 1989; Thayer et al., 2003; Chu et al., 2006; Lübken, et al., 2008.). Observations have also been made by a number of satellite experiments, most of them serendipitously (DeLand et al., 2006; Eremenko et al., 2005). Additional interest in mesospheric clouds stems from the unique conditions of cloud formation in the weakly ionized D-region (a 'dusty plasma'), and their close relationship with a mesospheric layer of strong radar reflectance referred to as polar mesospheric summer echoes (PMSE) (e.g. Rapp and Lübken, 2003a, b, 2004).

At least three factors are believed to control PMC formation: (1) temperature, (2) water vapor, and (3) meteoric smoke or some other nucleation source. The detailed role of water vapor has not yet been established, although it is clearly important in the cloud saturation and growth processes. There is now evidence that the clouds redistribute water vapor (Summers et al., 2001), which in turn could affect the ozone concentration and heat balance (Siskind et al., 2005). There are many open questions regarding cloud nucleation, microphysics (Rapp and Thomas, 2006), and the roles of chemistry, gravity waves, transport, and cosmic dust influx. Despite the sophistication of present-day modeling (e.g. Berger and Lübken, 2006), these uncertainties hamper our ability to understand the origin of the observed changes and we cannot project with confidence future changes. In short, we do not understand what causes a mesospheric cloud to form, or how it evolves. To establish the basis for new predictive PMC models, high-precision measurements of PMCs and key chemical constituents are required for various conditions of temperature, cosmic dust influx, and H_2O concentrations.

The Aeronomy of Ice in the Mesosphere (AIM) mission was launched from Vandenberg Air Force Base on April 25, 2007 becoming the first satellite mission dedicated to the study of PMCs. A Pegasus XL rocket placed the AIM satellite into a near circular (601 km apogee, 595 km perigee), 12:00 AM/PM sun-synchronous orbit. By measuring PMCs and the thermal, chemical and dynamical environment in which they form, AIM will quantify the connection between these clouds and the meteorology of the polar mesosphere. In the end, this will provide the basis for study of long-term variability in mesospheric climate and its relationship to global change. The results of AIM will be a rigorous test and validation of predictive models that then can reliably use past PMC changes and current data to assess trends as indicators of global change. This goal is being achieved by measuring PMC abundances, spatial distribution, particle size distributions, gravity wave activity, cosmic dust influx to the atmosphere and vertical profiles of temperature, H_2O, O_3, CH_4, and PMC extinction. CO_2 and NO retrievals are currently not operational, but these parameters will be available in future data versions.

The overall goal of AIM is to resolve why PMCs form and why they vary. The science team has established a set of six objectives designed to address the mission goal. The first objective is to understand the cloud microphysics, i.e. the relationship between temperature, water vapor and size distribution under a variety of conditions and times in the PMC season, and for different cloud types. The second objective is focused on assessing the role of atmospheric gravity waves in PMC formation. It is clear that waves are important because their presence is obvious in the many ground-based photographs of the clouds. The third objective addresses the question of the influence of temperature in controlling the length of the PMC season. Clearly, extremely low temperatures (on the order of 140 K or less) are essential because where the clouds form ~83 km above the surface, the pressure is one hundred thousand times less than at the surface and the air may be as much as a million times drier than surface desert air. The fourth objective addresses upper mesosphere H_2O chemistry and how it changes during the PMC season. As noted earlier, the clouds are known to be made up of water ice crystals and interactions between H_2O and O_3 and the role of solar Lyman-α radiation which controls H_2O at the cloud altitude needs to be understood. The fifth objective is to assess the sources of seed particles needed for PMC formation by providing a nucleation site to begin the particle growth process. The last objective combines results from the first five to validate coupled chemistry, dynamics and PMC microphysical models and to assess the ability to quantify long-term changes, and predict future changes in PMCs based on these models, historical data sets and AIM results.

The AIM experiment includes three instruments: the solar occultation for ice experiment (SOFIE), a solar occultation differential absorption radiometer covering the ultraviolet (UV) to infrared (IR) region; the cloud imaging and particle size experiment (CIPS), a panoramic UV imager; and the cosmic dust experiment (CDE), an in-situ cosmic dust detector. In this paper, we describe the AIM mission including the instruments and their data products, the overall mission implementation and early science results.

2. The AIM science instruments

2.1. Solar occultation for ice experiment (SOFIE)

SOFIE (Fig. 2) is performing satellite solar occultation measurements to determine vertical profiles of temperature, pressure, the abundance of five gaseous species (H_2O, O_3, CO_2, CH_4, and NO) and extinction at eleven wavelengths. Occultation measurements are accomplished by monitoring solar intensity as the satellite enters or exits the Earth's shadow. The ratio of solar intensity measured through the atmosphere (V) to the exoatmospheric solar intensity (V_{exo}) yields atmospheric transmissions, ($\tau = V/V_{exo}$), which are the basis for retrieving geophysical parameters. SOFIE uses differential absorption radiometry, with eight channels consisting of band pairs covering wavelengths (λ) from 0.292 to 5.316 μm (see Table 1). The SOFIE instrument approach uses 16 broad filters and is focused on a set of measurements needed to accomplish AIM science objectives. The instrument design is inherently simple having only one moving part, a 1 KHz chopper, which reduces risk and cost. This is in contrast to the more powerful, high spectral resolution

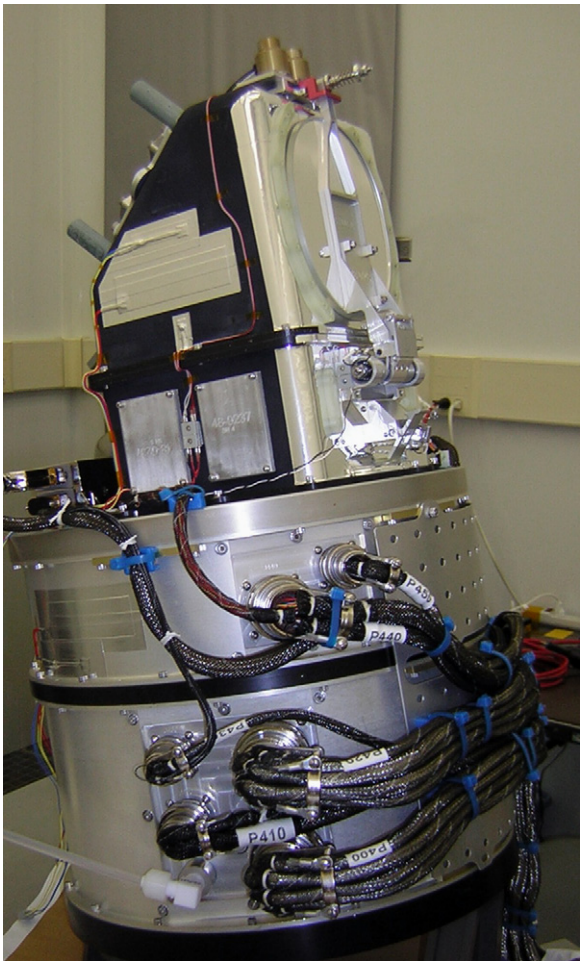

Fig. 2. SOFIE instrument.

Table 1
SOFIE channel characteristics

Channel	Band	Target[a]	Center λ (μm)	$G_{\Delta V}$
1	1	O_3 s	0.292	30
	2	O_3 w	0.330	
2	3	PMC s	0.867	300
	4	PMC w	1.037	
3	5	H_2O w	2.46	96
	6	H_2O s	2.618	
4	7	CO_2 s	2.785	110
	8	CO_2 w	2.939	
5	9	PMC s	3.064	120
	10	PMC w	3.186	
6	11	CH_4 s	3.384	202
	12	CH_4 w	3.479	
7	13	CO_2 s	4.324	110
	14	CO_2 w	4.646	
8	15	NO w	5.006	300
	16	NO s	5.316	

[a] s indicates strongly absorbing band, w denotes weakly absorbing band.

interferometer method such as that used by ACE which has broader scientific objectives but has higher data rates and somewhat reduced signal-to-noise (Eremenko et al., 2005). Also, the broad SOFIE spectral range from ~0.3 to 5 μm, a temporal resolution of <0.5 s and a S/N in the $>10^5$–10^6 range would be difficult to achieve with a high-spectral resolution instrument. Gordley et al. (1994, 2008) and Hervig et al. (2008a), provide details of the SOFIE instrument design, characteristics, calibration, retrieval methods and on-orbit performance in companion papers in this special issue.

Specific gases are targeted by measuring solar intensity in two wavelength regions; one where the gas is strongly absorbing and an adjacent region where the gas is weakly absorbing. SOFIE measures the strong and weak band radiometer signals (V_S and V_W) and the difference of these which is amplified by an electronic gain ($G_{\Delta V}$) to give a difference signal $\Delta V = (V_w - V_s)\ G_{\Delta V}$. An example of SOFIE band positions with respect to calculated transmission spectra for relevant gaseous absorbers and PMCs is shown in Fig. 3 for the H_2O channel. Note that the strong band H_2O absorption is more than 20 times stronger than for PMCs, making the SOFIE H_2O measurements immune to PMC contamination. While a single band measurement alone can be sufficient to retrieve gas mixing ratios in the lower mesosphere and stratosphere, SOFIE is characterizing the tenuous altitude regions where PMCs form and well above into the lower thermosphere. At these altitudes, atmospheric and gaseous abundances are low and the corresponding signals can approach typical noise levels. However, common mode optics and electronics errors are greatly reduced by measuring the difference in intensity between adjacent strong and weak absorption bands. Benefits are realized because a variety of atmospheric and instrumental effects are nearly identical in the strong and weak bands, and are therefore greatly reduced by differencing band pairs. Another benefit is that electronic gain can be applied to the difference signals, allowing the measurement precision to be enhanced to a level consistent with the detector noise. Six SOFIE channels are designed to measure gaseous signals, and two are dedicated to particle measurements. Particle measurements are also obtained from the gas channel weak bands. Measurements in two CO_2 bands are being used to simultaneously retrieve temperature and CO_2 mixing ratio (Gordley et al., 2008). SOFIE H_2O measurements are unaffected by PMCs, and temperatures are only impacted by very bright PMC layers ($\leqslant 3$ K uncertainty due to removal of PMC contamination of the signal). The O_3 and CH_4 measurements are affected by PMC contamination. This effect falsely increases O_3 mixing ratios by about 0.25 ppmv (on average) when PMCs are present. Because CH_4 measurements are severely impacted by PMCs and the abundance of CH_4 is very low above 75 km, SOFIE

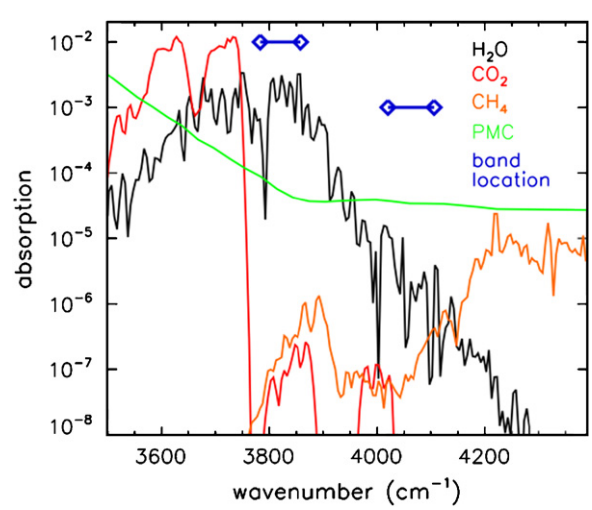

Fig. 3. Calculated transmission spectra for key absorbers near the PMC height within the SOFIE water vapor channel wavelength region.

CH_4 retrievals cease above 75 km (see Gordley et al., 2008). The SOFIE sun sensor provides measurements of atmospheric refraction angle with sub-arc second precision that are being used to retrieve temperature profiles at altitudes below about 50 km based on atmospheric refraction measurements.

2.1.1. SOFIE measurement geometry

SOFIE provides spacecraft sunset measurements at latitudes between about 65° and 85°S and sunrise measurements at latitudes between about 65°N and 85°N (see Gordley et al., 2008). SOFIE observes 15 sunrise and 15 sunset occultations per day, and consecutive sunrises or sunsets are separated by ~96 min in time or ~24° in longitude. The SOFIE field-of-view (FOV) at the tangent point is ~1.5 km vertical by ~4.4 km horizontal. The SOFIE measurement suite, consisting of 16 radiometer and 8 difference signal measurements, is sampled at 20 Hz, which corresponds to a vertical distance of ~145 m in the atmosphere. The vertical resolution of 1.5 km combined with the ~3 km s^{-1} solar sink or rise rate sets the natural frequency of the data set at ~2 Hz, which is the rate at which the FOV vertical dimension is swept through the atmosphere.

2.1.2. SOFIE instrument performance

SOFIE performance was characterized in laboratory calibration studies before launch and detailed characterizations have been completed in orbit. Laboratory calibration sequences addressed important instrument characteristics including measurement background and noise, FOV, response linearity, relative spectral response, time response, absolute gain, and difference signal gain. Because the basic measurements are ratios of signals used to determine atmospheric transmissions, absolute radiometric calibration is not important, except to ensure that the exoatmospheric solar view generates signals near the upper limit of the data acquisition system. Performance of the SOFIE measurement and retrieval system in-orbit is excellent in all cases with noise levels at or below laboratory values. The retrieval precision and altitude range based on data analysis thus far are summarized in Table 2. In all cases SOFIE performance meets or exceeds AIM science requirements. Note that SOFIE CO_2 and NO retrievals are currently not operational, but will be available in future data versions. Gordley et al. (2008) give a detailed description of the SOFIE measurement and retrieval characteristics.

2.1.3. SOFIE physical PMC properties

Hervig et al. (2008a) describe the use of SOFIE observations to identify PMCs and determine a variety of physical cloud properties. The reader is referred to this paper for a detailed discussion of the derivation of these properties. It includes a detailed review of relevant issues related to modeling SOFIE PMC signals such as the scattering regime, its effect on retrieval methodology, ice optical constants, and their temperature dependence. The unique combination of UV thru IR PMC measurements provides key information concerning the PMC size distribution. The size distribution retrievals assume the unimodal Gaussian form, which describes the concentration versus radius in terms of the total particle concentration (N), mode radius (r_m), and distribution width (Δr). Ice is identified using the measured extinction profiles at 3.064 and 3.186 μm wavelength considering the ice spectral signature and the measurement noise. SOFIE measurements are analyzed to determine the altitude dependence of ice particle mass density (M_{ice}), effective radius (r_e), particle shape as the axial ratio (AR) of a spheroid, and the parameters of a Gaussian size distribution. Uncertainties are estimated to be <11% for M_{ice}, <15% for r_e, and <20% for a typical AR values. Uncertainties in the Gaussian distribution parameters are estimated to be <25% for r_m and <40% for N and Δr (Hervig et al., 2008a). SOFIE results from the northern summer of 2007 are discussed below and in Hervig et al. (2008a, b).

Table 2
SOFIE retrieval characteristics

Retrieval	Measurement precision at 83 km (unless noted)	Altitude range (km)
T	0.2 K	40–95
O_3	11 ppbv	55–95
H_2O	70 ppbv	20–95
CH_4	5 ppbv (70 km)	20–75
PMC extinction (radiometers)	5×10^{-8} km^{-1}	Cloud altitude

2.2. Cloud imaging and particle size experiment (CIPS)

The CIPS instrument is a panoramic UV nadir imager operating at 265 nm with a 120° × 80° FOV and 5 × 5 km horizontal spatial resolution. The fundamental observation is scattered radiance from PMCs at 83 km altitude that is used to derive PMC morphology and cloud particle size information. The instrument provides multiple exposures of individual clouds at a variety of scattering angles in order to allow removal of the Rayleigh scattering component of the signal, determine cloud presence, provide the spatial morphology of the clouds, and constrain the parameters of cloud particle size and size distribution. The high-spatial resolution measurements of the variation of the Rayleigh scattered background also provides information on gravity wave activity in the 55-km region and small-scale variations in lower mesospheric ozone. More detail on the instrument, its measurements and data retrieval is provided in other papers in this special issue by Rusch et al. (2008) and Bailey et al. (2008).

2.2.1. CIPS instrument design

The CIPS instrument consists of an array of four cameras (Fig. 4) operating with a 15 nm passband centered at 265 nm. Each camera has an overlapping FOV and a pixel size at the nadir of ~2 km. The FOV of the camera system is 80° × 120°, centered at the sub-satellite point, with the 120° axis along the orbit track (Fig. 5). McClintock et al. (2008) in this issue provide a detailed discussion of the CIPS instrument concept, design, calibration, and on-orbit performance. Because of slant viewing, the spatial resolution increases to ~6.4 km near the edge of the FOV of the forward and aft cameras. The combination of images from the four cameras is referred to as a scene. CIPS records scenes of atmospheric and cloud radiance in the summer hemisphere from the terminator to ~40° latitude along the sunlit portion of the orbit. The near-polar orbit and cross-track FOV will cause the observation swaths to overlap at latitudes higher than about 70°, so that nearly the entire polar cap will be mapped daily by the 15-orbit per day coverage (see a CIPS daily mean image in Fig. 6). In the nominal pointing mode, the CIPS images extend poleward to about 85° latitude in each hemisphere.

Each camera has a focal ratio of 1.12, a focal length of 28 mm, a 25 mm lens diameter and includes an interference filter and a Charge Coupled Device (CCD) detector system. The throughput of the optical elements and their sizes are designed for a ±1% measurement precision of the background sunlit Earth. The custom UV filters were manufactured by Barr associates and centered at 265 nm. The CCD detectors are coupled with Hamamatsu V5181U-03 image intensifiers (40 mm diameter active area) and have 2048 × 2048 useful pixels that are electronically binned in 4 × 8 combinations for an effective 340 (cross track) × 170 (along track) pixel images. The signal in each pixel is

digitized to 12 bit resolution. On average, 26 images are produced per orbit in the summer polar region with special 'first light' images just beyond the terminator.

Imaging is achieved with this body-fixed camera assembly using an exposure time of 1 s, which, when combined with the FOV, yields the nadir spatial resolution of ~2 km. Between four and seven exposures of the same cloud volume are made during a satellite overpass, at a rate of one scene every 46 s. Each CCD is equipped with a digital signal processing (DSP) interface that incorporates a lossless Huffman compression algorithm, reducing data volume by about a factor of two. Therefore, each scene produces 523 Kbytes of data yielding approximately 18 Mbytes per orbit. The CIPS requirements and measured performance characteristics are listed in Table 3. Throughout the orbit, the CIPS instrument takes scenes at 43 s intervals. Due to the large FOV, this allows viewing the same region of the atmosphere at seven different scattering angles over a 258 s cadence. The seven measurements at seven different scattering angles define the PMC scattering phase function. The ~4 min duration between the seven measurements is small compared with ice decay lifetimes, which in the extreme case are likely limited by temperature fluctuations in the most rapidly varying wave motions (the Brunt-Väissala period which is ~5–6 min). Ice growth is much slower than ice decay, depending upon the small rate of water vapor deposition (Jensen and Thomas, 1994).

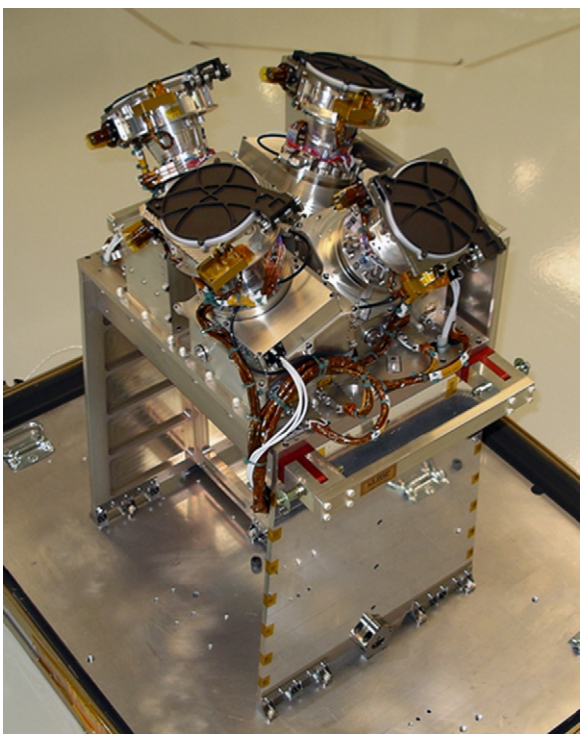

Fig. 4. CIPS Instrument.

2.2.2. CIPS PMC high-resolution structure

PMCs are identified as enhancements of brightness against the Rayleigh-scattered background coming from the lower mesosphere. Thomas et al. (1989a) proved the feasibility of this detection method using 273.5 nm data from the SBUV nadir-viewing spectrometer on board the NIMBUS 7 spacecraft. They showed that the brightest PMCs could be distinguished against the background despite the clouds under-filling the 150 × 150 km FOV. One key to detecting relatively weak PMCs is to observe at wavelengths where the Earth's albedo is at or near a minimum due to ozone absorption. The 265 nm central wavelength of CIPS was chosen because it represents a peak in ozone absorption, and therefore a minimum in the background originating from scattering of sunlight from air molecules. Estimates of the relative brightness of the NO fluorescence signal with respect to the Rayleigh scattering albedo at these wavelengths were found to be

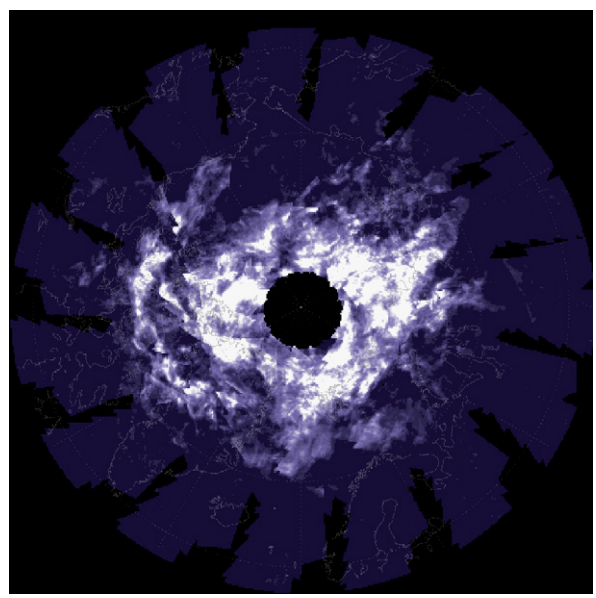

Fig. 6. CIPS daily mean image showing coverage for a full day of CIPS images on July 17, 2007. FOV overlap from one orbit to the next occurs at ~70°N. The lowest latitude in the plot is 58°N.

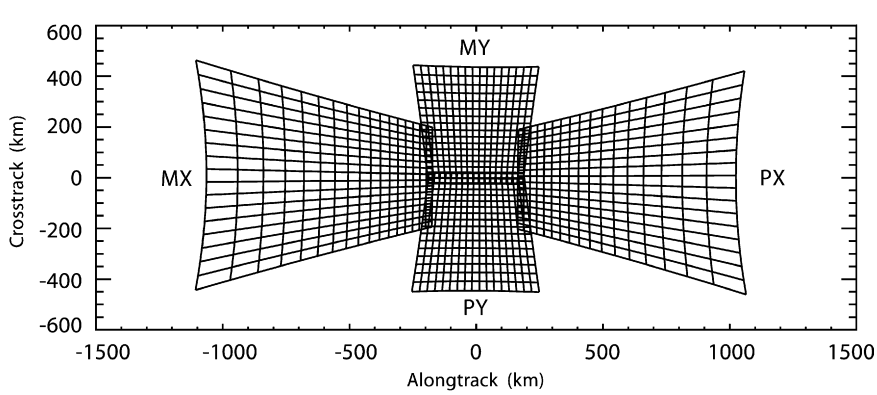

Fig. 5. CIPS FOV projected to 83 km. The satellite velocity vector direction is to the right.

Table 3
CIPS Requirements and performance

Parameter	Reqmt.	Design	Measured
Spatial resolution (nadir)	3.0 km	2.1 km	2.1 km
Absolute accuracy	15%	10%	10%
Precision (SNR for Earth albedo $= 2\times10^{-5}\,\mathrm{sr}^{-1}$)[1]	2.0	4.7	5.2

less than 1% of the background intensity and thus are negligible. This observed background radiance is generally limited by ozone to scattering in the vicinity of 55 km and above. A second key feature is the measurement of cloud brightness at small ($<35^\circ$) scattering angles that greatly enhances the cloud contrast with respect to the Rayleigh background because of the forward-scattering property of ice particles in the Mie regime.

CIPS observations at solar zenith angles (SZA) from 87° to about 94° (the 'shadow band') experience a reduction in background signal by at least a factor of 10 from full daylight brightness while the higher altitude PMCs remain at least 95% illuminated relative to an overhead sun condition. This results in greatly enhanced PMC contrast because the background is mostly in darkness. The shadow band is roughly 700 km wide and centered on the location of SOFIE coincident observations. As discussed earlier, we refer to that location as the 'Common Volume' because both CIPS and SOFIE observe the same volume of atmosphere within a period of 6 min.

The CIPS high spatial resolution provides the ability to measure small structures in PMCs and in the Rayleigh-scattered background. When clouds are present, the CIPS measurements yield GW wavelengths, extent, and morphology at the cloud height. From these data, the impact of wave dynamics on PMC formation and destruction are being derived. The GWs provide significant energy input to the mesosphere and are a large driver of mesospheric 'weather'. In addition, during cloud-free times, i.e. when cloud signatures are below the CIPS detection threshold, CIPS will measure structure in the 55 km region. Because the bright PMCs are confined to a summertime period about 12–13 weeks long, and mostly to a region poleward of the Arctic and Antarctic circles (Thomas and Olivero, 1989), the CIPS observing strategy allows for adequate collection of data from cloud-free regions, both before and after the cloud 'season', and at lower latitudes during the season ($<55^\circ$). These regions are being used to characterize signatures of small-scale wave transport of energy from the lower atmosphere—gravity waves, as well as planetary scale waves.

Gravity wave effects on background CIPS signals occur because these waves create temperature changes in the atmosphere that alter ozone which is the primary absorber of scattered sunlight observed by CIPS. Because the ozone chemistry is highly temperature dependent, the ozone density responds rapidly to the imposed temperature fluctuations (the photochemical time constant is on the order of a minute at 55 km (Brasseur and Solomon, 1986). The resulting effect on the UV albedo in the highly absorbing Hartley bands of ozone is easily found from a single-scattering calculation to be linearly dependent upon the ozone perturbation. Multiple scattering is negligible at 265 nm. Wave amplitudes as small as 1–2 K at 55 km will cause approximately a 3% perturbation in background signal, which is a change easily detectable by CIPS above the otherwise smoothly varying background due to Rayleigh scattering.

Clouds are identified by their large angular-dependent scattering signature which is a well-established property of PMC particles (Thomas and McKay, 1986; Gumbel and Witt, 1998). Cloud ice particles scatter light predominantly in the forward direction. This effect is more pronounced for brighter clouds, or more specifically clouds having larger particle size. The background Rayleigh-scattered sunlight follows a well-known variation with scattering angle that is symmetric about 90° scattering angle. Any brightness enhancement that shows forward scattering behavior can be identified as a PMC, and not an underlying background irregularity. This leads to a methodology for separation of the signature of the cloud albedo from that of the underlying background. The scene recorded by CIPS includes a Rayleigh-scattered sunlight background at altitudes near 55 km and Mie-scattered sunlight by PMC particles at ~83 km. The magnitude of the background is controlled by ozone which absorbs radiation along the path. For SZA away from the terminator, ozone limits contributions to the observed CIPS radiance to altitudes only above 50 km. The crux of the CIPS measurement interpretation is determining the PMC signal by subtracting the Rayleigh background. CIPS determines the scattering phase function by imaging the same point in space at multiple angles. In one approach, the background signal can be inferred using the difference between cloud and molecular scattering phase functions. Alternatively, the background can be calculated given profiles of temperature, pressure, and ozone taken from SOFIE measurements within the common volume (CV). The CIPS instrument is sensitive to ice particles with radii greater than ~30 nm. Under typical observing conditions, assuming a 1 km vertical cloud layer thickness, a Gaussian particle size distribution of 14 nm width and a mode radius of 45 nm, the CIPS detectability level (i.e. three times the noise) is 102 cm^{-3}. Under optimal conditions, i.e. in the CV (discussed later in Section 3) where the Rayleigh background is greatly reduced, the detectability is 25 cm^{-3}.

Given the water–ice composition (Hervig et al., 2001) and the shape factor of the irregular ice particles (see Rapp et al., 2007 for further discussion of the shape issue) the CIPS angular distributions of brightness at a single wavelength yield column mass, surface area, and mean particle size. These results allow correlation of CIPS PMC properties with SOFIE PMC extinction, temperature, water vapor, and other atmospheric parameters. The particle size distribution within the CV (discussed later in Section 3) can be more constrained by combining the CIPS observations with SOFIE measurements of PMC optical depths in the CV rather than using the data from one instrument alone.

2.3. Cosmic dust experiment (CDE)

CDE is an impact dust detector based on thin (28 μm) permanently polarized polyvinylidine fluoride (PVDF) foil sensors (Simpson and Tuzzolino, 1985). It is included in the AIM payload to monitor the variability of micron sized grains of cosmic dust influx into our atmosphere at the satellite altitude of 600 km. Since the time for an incoming micrometeoroid to travel from 600 km to the PMC region is very short (<1 min), CDE measurements directly indicate the influx of cosmic matter to the mesosphere where it ablates to become meteoric smoke. Meteoric smoke particles are considered to be the most likely candidate to form PMC nucleation sites (Rapp and Thomas, 2006). The spatial scale of the flux of the background micrometeoroids, as opposed to the named meteor streams (Fentzke and Janches, 2008), is comparable to the entire Earth; hence changes in dust influx to the mesosphere are expected to occur over a complete hemisphere.

CDE observations integrated over several days are expected to show the temporal variability of the cosmic dust influx that could influence the formation of PMCs. The cosmic dust delivered to the mesosphere is most likely ablated to particle radii of ~0.2 nm

(Bardeen et al., 2008), which coagulate to PMC nucleation sites of ~1 nm. Recent results from global-scale models reveal that variations in the influx of meteoric material can dramatically affect the availability of nucleation sites in the polar summer mesosphere (Megner et al., 2008; Bardeen et al., 2008). Although the availability of nucleation sites depends strongly on equatorward transport from the polar summer mesosphere, large uncertainties exist in the models regarding total influx of material, the initial radius of the dust and the coagulation efficiency. The temporal variability of meteoric material measured by CDE will be used with observed variations in PMCs and model studies to assess the role that extraterrestrial forcing plays in PMC formation and variability. Such studies will involve sorting out other sources of variability of ice properties, and thus will probably require several PMC seasons to build up an adequate data base.

PVDF dust detectors have been flown on the VEGA 1 and 2 missions to comet Halley (Simpson et al., 1986), on the STARDUST mission to comet Wild 2 (Tuzzolino et al., 2004), on the Cassini mission to Saturn (Srama et al., 2004), and the Earth observing ARGOS satellite (Tuzzolino et al., 2005). A copy of the CDE instrument is on the New Horizons mission to Pluto (Horanyi et al., 2007). PVDF sensors have many advantages: they require no bias or high accelerating voltages, they are electrically, mechanically and thermally stable, radiation resistant, do not respond to charged particles, and can measure very high rates of dust impacts. The disadvantage of this sensor is that the charge signal generated by an impact is a function of both the mass and the velocity of the dust grain. Hence, in the analysis of the CDE data one has to assume a characteristic meteorite speed and average flight angle with respect to the local zenith in order to infer meteorite mass. A similar approach was used in the analysis of the impact craters on the long duration exposure facility (LDEF) (Love and Brownlee, 1993). The charge Q (in units of electron charge) generated by a particle with mass m, (in units of grams), and relative velocity v (measured in km/s) is: $Q = 3.8 \times 10^{17} m^{13} v^3$. The size of an individual PVDF detector ultimately determines the mass threshold as well as the expected impact rate. The capacitance of the PVDF film is proportional to its surface area and, in turn, the electronic noise level is set by the capacitance. The required mass (charge) threshold ultimately sets the maximum size of an individual PVDF patch.

The CDE goal to measure an expected impact rate of $\geqslant 100$ hits/week requires a mass threshold of $\leqslant 4 \times 10^{-12}$ g and a total sensitive surface area of $\geqslant 0.1\ \mathrm{m}^2$. To meet this requirement CDE (Fig. 7) consists of 12 active PVDF patches with surface areas of $85\ \mathrm{cm}^2$ each. In addition, there are two other sensors (identical to the front side patches), on the back side of CDE that cannot be hit by dust. These reference detectors are being used to measure the noise background. The CDE dynamic range provides mass resolutions within a factor of $\leqslant 3$ in the mass range of 4×10^{-12} g $\leqslant m \leqslant 4 \times 10^{-9}$ g covering an approximate size range in particle radius of $0.8\ \mu\mathrm{m} \leqslant a \leqslant 8\ \mu\mathrm{m}$.

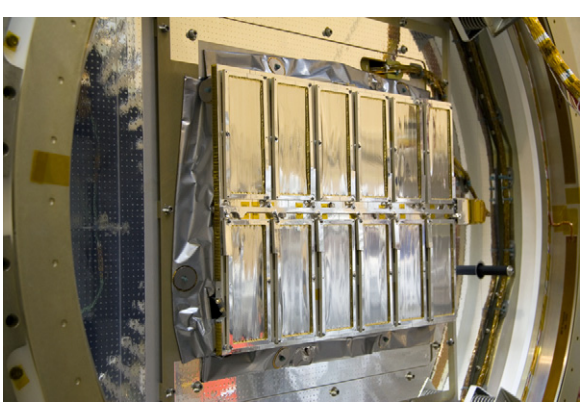

Fig. 7. CDE sensors mounted on the top of the spacecraft. Each patch of the 12 active PVDF sensors has a surface area of about $85\ \mathrm{cm}^2$. The panel is mounted to point towards the local zenith direction at all times, minimizing the impact rates from orbital debris.

Each of the 14 sensors has an adjustable threshold to optimize CDE operations. To follow the possible degradation of its performance due to ageing, CDE has onboard calibration capabilities for its electronics. Internal signals can be injected in each of the 14 channels with amplitudes covering its entire dynamical range. Each dust hit generates a science event, where the time, channel number and the impact charge are recorded, in addition to all relevant housekeeping data. Using appropriate averages this can be turned into a time-dependent global map to show the possible spatial and temporal variability of the amount of cosmic dust entering the atmosphere.

3. AIM observation scenario and the CV

Occultation and imaging measurements have inherent benefits, but also present unique challenges to measurement interpretation. For example, CIPS observations in the general nadir direction offers high horizontal resolution (5 km) but essentially no height information, while SOFIE, which views on the limb, provides high vertical resolution (1.5 km) with relatively coarse horizontal resolution (290 km along the limb by 4 km across-limb). Combining observations where the two measurements spatially overlap in what we call the CV, allows mitigation of certain measurement limitations and offers opportunities to increase the information provided by each data set. The SOFIE tangent point location and footprint defines the AIM CV. CIPS views the CV roughly 6 min before or after SOFIE, which is well under the 20–30 min time scale of PMC variability (e.g. Gadsden, 1982, 1985). Thus, the AIM observation scenario provides spatially coincident CIPS and SOFIE observations on every orbit. Limb retrievals traditionally assume that all atmospheric absorbers are distributed in a spherically symmetric fashion. While spherical symmetry is an appropriate assumption in most cases when measuring gaseous species, PMCs can vary over smaller scales than accommodated by the limb path geometry (Fritts et al., 1993). If ignored, cloud inhomogeneity can result in fundamental errors, although the sign of the errors is at least predictable. Variable cloud cover will always result in an underestimate of the instantaneous cloud extinction because the measurement inversion assumes that the absorber occupies the entire tangent path length. A cloud within the line-of-sight (LOS) but not at the tangent point will always be assigned an erroneously low altitude because its position is assumed to be at the tangent point. In addition, the clouds will have relatively low extinctions because the LOS intercepts them at off-tangent angles resulting in reduced path length through the cloud. Hervig et al. (2008a) offer a preliminary assessment of these effects in SOFIE observations, and show that PMCs detected at anomalously low altitudes have lower extinction that is consistent with isolated clouds within the near or far extent of the LOS. SOFIE measurement interpretation is addressing these issues using CIPS images to provide the detailed horizontal distribution of PMCs.

The AIM spacecraft accommodates CV measurements by transitioning from sun pointing during the SOFIE occultation to an Earth inertial pointing mode for the CIPS imaging period. This orientation also allows SOFIE and CIPS to view though the same 2-D plane, with CIPS viewing multiple angles as it passes over the occultation tangent point. Earth rotation (~1°, typically <50 km) will prevent perfectly coincident planar viewing, but this is

unimportant considering the natural horizontal resolution of the SOFIE sample volume (~290 km along the limb path).

4. Spacecraft status

All AIM spacecraft systems have been functioning nominally since launch on April 25, 2007 except for the command receiver. The receiver has had periods of intermittent command signal rejection, but the AIM Flight Operations team has been able to successfully work around these difficulties. Full science operations began on May 22, 2007. Routine science data processing started in February 2008. All data products are available to the public via the internet at the main AIM webpage at www.aim.hamptonu.edu.

5. Early science results

Brief highlights of early science findings are presented in this section and more results as well as additional details are contained in other AIM papers in this special issue. AIM is providing the first global scale view of PMCs in the polar cap region with a spatial resolution that is unprecedented. Results show that the clouds are highly variable from orbit to orbit and day-to-day. Figs. 8 and 9 show daily mean CIPS images on two successive days in late June and early July 2007. As discussed above, these images have had the Rayleigh background signal removed so that what remains is only PMC signatures. Further details of how the background removal is accomplished are provided in papers in this issue by Rusch et al. (2008) and Bailey et al. (2005). Note the significant increase in the number of clouds from June 30 to July 1st. The clouds on June 30th are not as bright and cover a much smaller area than on the next day. Also note the very pronounced void in the cloud field in the first quadrant of Fig. 9. We refer to this feature as an ice void. These features are currently unexplained but are common occurrences in the CIPS images. Ice minima appear in satellite PMC occurrence frequency time series during the season as reported by Bailey et al. (2005) and they also occur in the LIMA model frequency of occurrence seasonal and latitudinal distribution (Berger and Lübken, 2006).

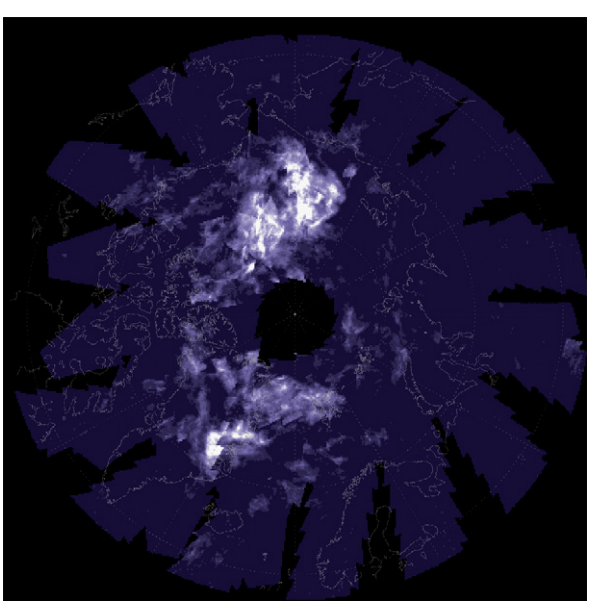

Fig. 8. CIPS daily mean image for June 30, 2007. The lowest latitude in the plot is 58°N.

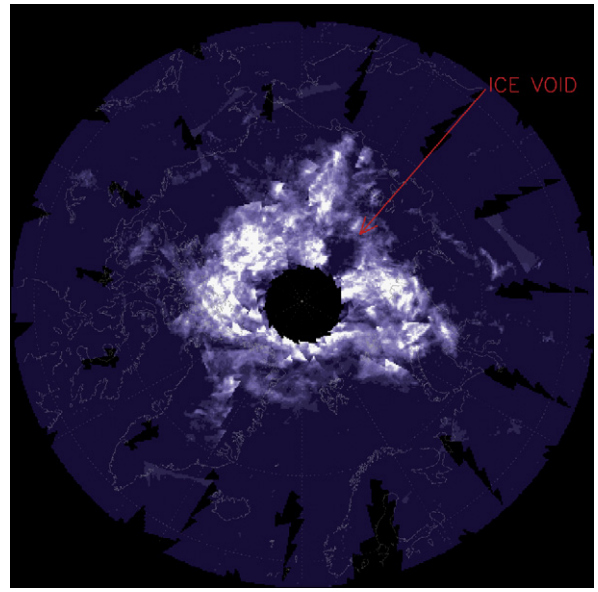

Fig. 9. CIPS daily mean image for July 1, 2007. Red arrow shows the location of the ice void. The lowest latitude in the plot is 58°N.

CIPS however, is the first instrument with sufficient horizontal resolution and a global scale view to show the true spatial extent and variability of these voids. They could be caused by energy deposition (heating) through gravity wave breaking, but they may also occur due to turbulent mixing from vertically displaced air (either by convective instability or also gravity wave breaking). Ice voids appear in circular or oval shapes with diameters that vary from ten to several hundred kilometers or greater. Rusch et al. (2008) discuss these features in more detail. These structures bear a startling similarity to those seen in tropospheric clouds and suggest that the mesosphere may share some of the same dynamical processes responsible for weather near Earth's surface. If this similarity holds up under further analysis, it could lead to a different view of mechanisms responsible for PMC formation and variability than existed before AIM was launched.

The multi-wavelength SOFIE observations are shedding new light on PMCs because of their extremely high precision and signal-to-noise. SOFIE measurement latitudes ranged from ~66 to 76°N during the 2007 northern PMC season, with an average latitude of 68.9°N for all PMC observations. While previous instruments suggested that PMCs are present about half the time near 70°N, SOFIE now shows that they are nearly always present at these latitudes during the PMC season. This result is consistent with radar observations near 70°N which indicate a nearly continual existence of PMSE, which are generally considered to be indirectly caused by the presence of ice. The SOFIE ice extinction detection threshold is 15–200 times below that of previous instruments, including lidars. In addition, it contains channels located at the peak in the ice absorption spectrum (~3 μm wavelength) where PMC extinction is ~100 times greater than for surrounding NIR and IR wavelengths. Hervig et al. (2008b) compare a time series of SOFIE ice occurrence frequency to SME and HALOE results. They check their results by downgrading SOFIE sensitivity to be consistent with HALOE and SME and find good agreement with results from these experiments, thus confirming that the lower ice frequencies recorded by the older satellites were a result of reduced sensitivity.

The time versus height cross-section of SOFIE H_2O in Fig. 10 illustrates the development of water vapor in the PMC environment during the 2007 northern cloud season. The measurement

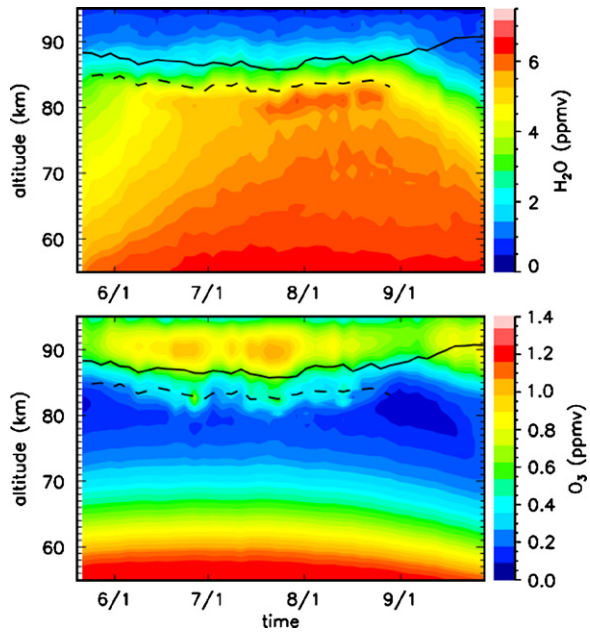

Fig. 10. Time–height cross-section of SOFIE H_2O and O_3 observations for the 2007 northern polar summer. Mesopause altitude (solid line) and the altitude of peak ice extinction (dashed line) are also indicated.

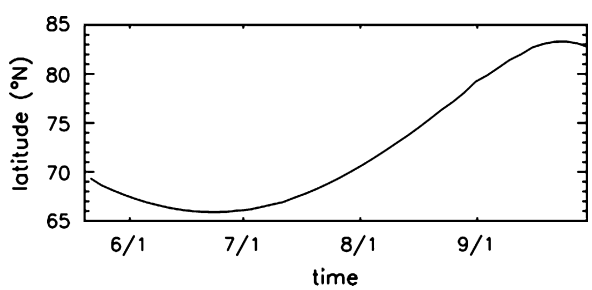

Fig. 11. The SOFIE measurement latitude track for the 2007 northern hemisphere summer season.

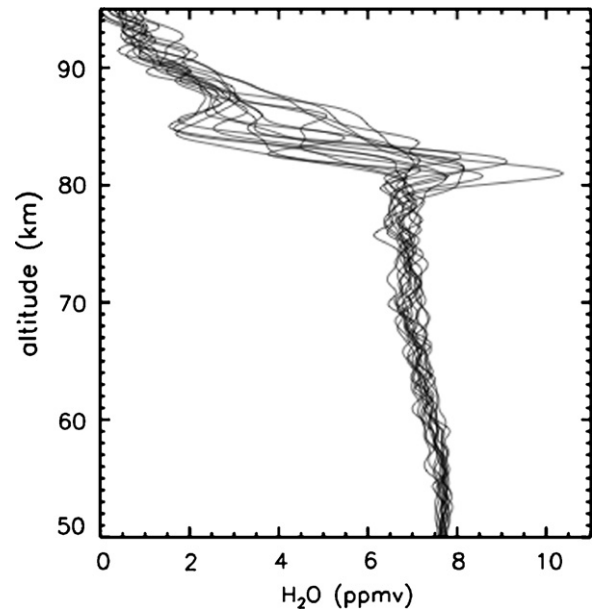

Fig. 12. SOFIE mesospheric water vapor profiles on August 12, 2007.

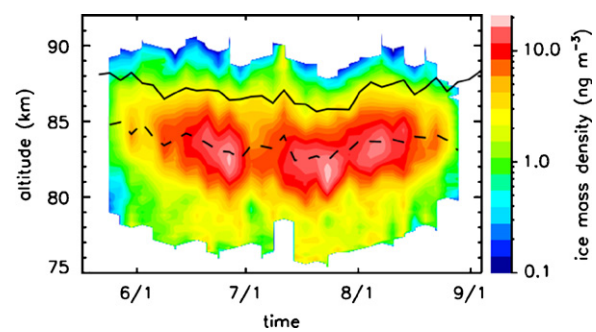

Fig. 13. SOFIE altitude versus time cross-section of ice mass density showing that the mesospheric ice extends over a broad altitude range. The solid line is the mesopause and the dashed line is the location of peak PMC extinction.

latitude time evolution for the season is shown in Fig. 11. Water vapor, an essential gas for PMC formation, is measured at a vertical resolution of 1.5 km and precision of 70 ppbv at PMC altitudes (Table 2). The seasonal evolution of water vapor is characterized by a rapid mixing ratio rise in the beginning of the summer and a steady increase after that time which is consistent with vertical transport due to upwelling (Summers et al., 2001). Reduced H_2O above ~80 km is consistent with a balance between upwelling and loss to PMC formation and to photolysis. SOFIE O_3 observations also shown in Fig. 10 indicate a mesospheric ozone minimum at about 81 km altitude at the beginning and end of the season and near 79 km throughout most of the season, with a peak observed near 90 km. O_3 enhancement is observed at altitudes from roughly 80–95 km during times that ice is present. While O_3 is affected by PMC contamination below ~90 km, the observations at higher altitudes are robust. For example, at 92 km the mixing ratio increases from 0.8 ppmv on 22 May to ~1.1 ppmv by 11 July, returning to ~0.8 ppmv by 15 August. This change in ozone is consistent with the suggestion by Siskind et al. (2005) that ozone should be enhanced above the ice layer due to dehydration by PMCs resulting in lowered HO_x. These observations of highly transient features, combined with the other SOFIE products are giving a first-time detailed look at the physics of PMCs.

An example of the quality of the underlying H_2O profiles is demonstrated in Fig. 12 which shows all observations for August 12, 2007. The decline in H_2O above ~80 km is generally consistent with loss of H_2O due to photolysis and to ice growth. Several profiles indicate pronounced dehydration near 85 km, which is near the altitude where PMC formation is expected. Enhanced H_2O is observed near 80 km where PMCs are generally thought to sublimate. It should be noted that H_2O profiles measured by SOFIE are of very high quality because as noted earlier, there is no PMC contamination in the signal thus allowing retrieval of H_2O directly in the presence of a PMC without any required corrections. This is a significant advantage and step forward.

SOFIE has also demonstrated that mesospheric ice exists as a continuous layer extending from ~80 km altitude to the mesopause (~87 km) and often higher, as shown in Fig. 13. A typical observed temperature profile that defines the mesopause on July 1, 2007 is shown in Fig. 14. This continuous layer view is supported by model predictions (von Zahn and Berger, 2003; Rapp and Thomas, 2006), but is in contrast with previous measurements that were not sensitive enough to detect the most tenuous ice populations. The SOFIE results now confirm a previously theorized but never before directly observed population of small ice particles in the altitude region above the main

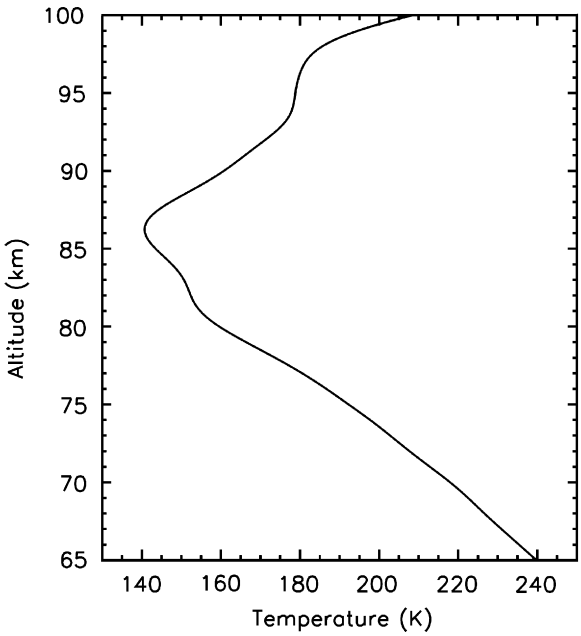

Fig. 14. A typical SOFIE temperature profile on July 1, 2007 at 66°N, 86.8°E showing the mesopause location.

PMC layer that are widely believed to be the indirect cause of PMSEs (see e.g. Rapp and Lübken, 2003a, b, 2004).

These results represent only a few of the findings about the properties of PMCs that have come from the first northern hemisphere season of observations. AIM has also completed observations of the first southern hemisphere season and already conventional ideas about inter-hemispheric differences in cloud properties are being challenged. The mission is providing high-quality data on particle size, size variation with altitude, particle shape and its altitude dependence, characteristics that describe the onset and end of the PMC season, the interplay between particles, water vapor and temperature, brightness variability over the entire polar cap region and space and time variability. The high sensitivity and spatial resolution provided by the AIM instruments is providing a rich data base to address all six AIM objectives and to answer the question of why these clouds form and vary.

6. Summary

Much has been learned about PMCs from hundreds of ground-based and rocket-borne measurements and observations from a number of satellite missions dating back 27 years. Most of the satellite studies were serendipitous in the sense that they were not conceived or designed to address PMC phenomena. AIM is the first mission dedicated to the exploration of PMCs. All systems designed to run the satellite are functioning as planned except for the command receiver and work arounds have been established for this subsystem. All instruments are functioning nominally. The appropriate mix of measurement capabilities and orbit parameters has been brought together to answer the fundamental question of why these clouds form and vary. The three science instruments are providing data needed to address a series of six objectives formulated by the AIM science team. Initial science results from the mission have advanced our understanding of PMC properties, variability, and spatial distribution after just one northern hemisphere season. The presence of voids in the ice layer observed by CIPS appears to be similar to a tropospheric weather phemenon and if true, it adds a potentially new mechanism that must be understood in addressing the question of why these clouds form and vary.

Acknowledgements

The authors acknowledge the many contributions of expertise, time, talent, and dedication given to the mission by the team of engineers, scientists, and managers of organizations supporting AIM at Hampton University, the University of Colorado Laboratory for Atmospheric and Space Physics, the Space Dynamics Laboratory of Utah State University, Orbital Sciences Corporation, GATS, Incorporated, the Goddard Space Flight Center and the Kennedy Space Center. Special thanks is given to the NASA Headquarters AIM Program Executive, Victoria Elsbernd and the AIM Program Scientist, Mary Mellott for their exceptional contributions to AIM through their sincere and extraordinary dedication to the success of this mission right from its inception. We also thank the AIM flight operations team at LASP, Orbital Sciences Corporation and GATS, Inc., for their commitment to excellence and their duty beyond the reasonable at times in order to make the mission succeed. It would not have been possible to present the exceptional data in this and other AIM papers in this special issue without the support of these individuals and organizations. Funding for the AIM mission was provided by NASA's Small Explorers Program under contract NAS5-03132.

References

Bailey, S.M., Merkel, A.W., Thomas, G.E., Rusch, D.W., Carstens, J.N., 2005. Observations of polar mesospheric clouds by the student nitric oxide explorer. Journal of Geophysical Research 110, D13202, (10.1029/2004JD005422).

Bailey, S.M., Thomas, G.E., Rusch, D.W., Merkel, A.W., Jeppesen, C.D., Carstens, J.N., Randall, C.E., McClintock, W.E., Russell III, J.M., 2008. Phase functions of polar mesospheric cloud ice as observed by the CIPS instrument on the AIM satellite. Journal of Atmospheric Solar Terrestrial Physics, this issue, doi:10.1016/j.jastp.2008.09.039.

Bardeen, C.G., Toon, O.B., Jensen, E.J., Marsh, D.R., Harvey, V.L., 2008. Numerical simulations of the three-dimensional distribution of meteoric dust in the mesosphere and upper stratosphere. Journal of Geophysical Research 113, D17202, doi:10.1029/2007JD009515.

Berger, U., Lübken, F.-J., 2006. Weather in mesospheric layers. Geophysical Research Letters 33, L04806, (10.129/2005GL02481).

Brasseur, G., Solomon, S., 1986. Aeronomy of the Middle Atmosphere, second ed. D. Reidel Publishing Company (pbk.).

Chu, X., Espy, P.J., Nott, G.J., Diettrich, J.C., Gardner, C.S., 2006. Polar mesospheric clouds observed by an iron Boltzmann lidar at Rothera (67.5°S, 68.0°W), Antarctica from 2002 to 2005: properties and implications. Journal of Geophysical Research 111, D20213, (10.1029/2006JD007086).

DeLand, M.T., Shettle, E.P., Thomas, G.E., Olivero, J.J., 2006. A quarter-century of satellite PMC observations. Journal of Atmospheric and Solar-Terrestrial Physics 68, 9–29.

DeLand, M.T., Shettle, E.P., Thomas, G.E., Olivero, J.J., 2007. Latitude-dependent long-term variations in polar mesospheric clouds from SBUV version 3 PMC data. Journal of Geophysical Research 112, D10315, (10.1029/2006JD007857).

Eremenko, M.N., Petelina, S.V., Zasetsky, A.Y., Karlsson, B., Rinsland, C.P., Llewellyn, E.J., Sloan, J.J., 2005. Shape and composition of PMC particles derived from satellite remote sensing measurements. Geophysical Research Letters 32, L16S06, (10.1029/2005GL023013).

Fentzke, J.T., Janches, D., 2008. A semi-empirical model of the contribution from sporadic meteoroid sources on the meteor input function in the MLT observed at Arecibo. Journal of Geophysical Research 113, A03304, (10.1029/2007JA012531).

Fritts, D.C., Isler, J.R., Thomas, G.E., Andreassen, O., 1993. Wave breaking signatures in noctilucent clouds. Geophysical Research Letters 20, 2039–2042.

Gadsden, M., 1982. Noctilucent clouds. Space Science Reviews 33, 279–334.

Gadsden, M., 1985. Observations of noctilucent clouds from North-West Europe. Annales Geophysicae 3, 119–126.

Goldberg, R.A., Fritts, D.C., Schmidlin, F.J., Williams, SB.P., Croskey, C.L., Mitchell, J.D., Friedrich, M., Russell, J.M., Blum, U., Fricke, K.H., 2006. The MaCWAVE program to study gravity wave influences on the polar mesosphere. Annales Geophysicae 24, 1159–1173.

Gordley, L.L., Marshall, B.T., Chu, D.A., 1994. LINEPAK: algorithms for modeling spectral transmittance and radiance. JQSRT 52, 563.

Gordley, L.L., Hervig, M.E., Fish, C., Russell III J.M., Bailey, S., Cook, J., Hansen, S., Shumway, A., Paxton, G., Deaver, L., Marshall, T., Burton, J., Magill, B., Brown, C.,

Thompson, E., Kemp, J., 2008. The solar occultation for ice experiment. Journal of Atmospheric and Solar-Terrestrial Physics, this issue, doi:10.1016/j.jastp.2008.07.012.
Gumbel, J., Witt, G., 1998. In situ measurements of the vertical structure of a noctilucent cloud. Geophysical Research Letters 25 (4), 493–496.
Hansen, G., Serwazi, M., von Zahn, U., 1989. First detection of a noctilucent cloud by lidar. Geophysical Research Letters 16, 1445–1448.
Hervig, M., Thompson, R.E., McHugh, M., Gordley, L.L., Russell, J.M., Summers, M.E., 2001. First confirmation that water ice is the primary component of polar mesospheric clouds. Geophysical Research Letters 38, 971–974.
Hervig, M.E., Gordley, L.L., Stevens, M.H., Russell III, J.M., Bailey, S.M., Baumgarten, G., 2008a. Interpretation of SOFIE PMC measurements: cloud identification and derivation of mass density, particle shape, and particle size. Journal of Atmospheric and Solar-Terrestrial Physics, this issue, doi:10.1016/j.jastp.2008.07.009.
Hervig, M.E., Gordley, L., Russell III, J.M., Bailey, S., 2008b. SOFIE PMC observations during the northern summer of 2007. Journal of Atmospheric and Solar-Terrestrial Physics, this issue, doi:10.1016/j.jastp.2008.08.010.
Horanyi, Hoxie, V., James, D., Poppe, A., Bryant, C., Grogan, B., Lamprecht, B., Mack, J., Bagenal, F., Batiste, S., Bunch, N., Chantanowich, T., Christensen, F., Colgan, M., Dunn, T., Drake, G., Fernandez, A., Finley, T., Holland, G., Jenkins, A., Krauss, C., Krauss, E., Krauss, O., Lankton, M., Mitchell, C., Neeland, M., Resse, T., Rash, K., Tate, G., Vaudrin, C., Westfall, J., 2007. The student dust counter on the new horizons mission. Space Science Reviews, (10.1007/s11214-007-9250-y).
Jensen, E.J., Thomas, G.E., 1994. Numerical simulations of the effects of gravity waves on noctilucent clouds. Journal of Geophysical Research 99, 3421–3430.
Leslie, R.J., 1885. Sky glows. Nature 33, 245.
Love, S.G., Brownlee, D.E., 1993. A direct measurement of the terrestrial mass accretion rate of cosmic dust. Science 262, 550–553.
Lübken, F.J., 1999. Thermal structure of the Arctic summer mesosphere. Journal of Geophysical Research 104 (D8), 9135–9149.
Lübken, F.-J., Baumgarten, G., Fiedler, J., Gerding, M., Höffner, J., Berger, U., 2008. Seasonal and latitudinal variation of noctilucent cloud altitudes. Geophysical Research Letters 35, L06801, (10.1029/2007GL032281).
McClintock, W.E., Rusch, D.W., Thomas, G.E., Merkel, A.W., Lankton, M.R., Drake, V.A., Bailey, S.M., Russell III, J.M., 2008. The cloud imaging and particle size experiment on the aeronomy of ice in the mesosphere mission: instrument concept, design, calibration, and on-orbit performance. Journal of Atmospheric and Solar-Terrestrial Physics, this issue.
Megner, L., Siskind, D.E., Rapp, M., Gumbel, J., 2008. Global and temporal distribution of meteoric smoke: a two-dimensional study. Journal of Geophysical Research 113, D03202, (10.1029/2007JD009054).
Rapp, M., Lübken, F.-J., 2003. On the nature of PMSE: electron diffusion in the vicinity of charged particles revisited. Journal of Geophysical Research 108, (10.1029/2002JD002857, eid:8437).
Rapp, M., Lübken, F.-J., 2003b. On the nature of PMSE: electron diffusion in the vicinity of charged particles revisited. Journal of Geophysical Research 108, (10.1029/2002JD002857, eid: 8437).
Rapp, M., Lübken, F.–J., 2004. Polar mesosphere summer echoes (PMSE): review of observations and current understanding. Atmospheric Chemistry and Physics 4, 2601–2633.
Rapp, M., Thomas, G.E., 2006. Modeling the microphysics of mesospheric ice particles: assessment of current capabilities and basic sensitivities. Journal of Atmospheric and Solar-Terrestrial Physics 68, 715–744.
Rapp, M., Thomas, G.E., Baumgarten, G., 2007. Spectral properties of mesospheric ice clouds: evidence for nonspherical particles. Journal of Geophysical Research 112, D03211, (1029/2006JD007322).
Rusch, D.W., Thomas, G.E., McClintock, W., Merkel, A.W., Bailey, S.M., Russell III, J.M., Randall, C.E., Jeppesen, C., Callan, M., 2008. The cloud imaging and particle size experiment on the aeronomy of ice in the mesosphere mission: cloud morphology for the northern 2007 season. Journal of Atmospheric and Solar-Terrestrial Physics 7, 7, this issue.
Simpson, J.A., Tuzzolino, A.J., 1985. Polarized polymer films as electronic pulse detectors of cosmic dust particles. Nuclear Instruments and Methods A236, 187–202.
Simpson, J.A., et al., 1986. Dust counter and mass analyzer (DUCMA) measurements of comet Halley's coma from VEGA spacecraft. Nature 321, 278–280.
Siskind, D.E., Stevens, M.H., Englert, C.R., 2005. A model study of global variability in mesospheric cloudiness. Journal of Atmospheric and Solar-Terrestrial Physics 67 (5), 429–519.
Srama, R., et al., 2004. The Cassini cosmic dust analyzer. Space Science Reviews 114 (1–4), 465–518.
Summers, M.E., et al., 2001. Discovery of a water vapor layer in the Arctic summer mesosphere: implications for polar mesospheric clouds. Geophysical Research Letters 28, 3601.
Taylor, M.J., Gadsden, M., Lowe, R.P., Zalcik, M.S., Brausch, J., 2002. Mesospheric cloud observations at unusually low latitudes. Journal of Atmospheric and Solar-Terrestrial Physics 64, 991–999.
Thayer, J.P., Rapp, M., Gerrard, A.G., Gudmundsson, E., Kane, T.J., 2003. Gravity-wave influences on Arctic mesospheric clouds as determined by a Rayleigh lidar at Søndrestrøm, Greenland. Journal of Geophysical Research 108 (D8), 8449, (10.1029/2002JD002363).
Thomas, G.E., McKay, C.P., 1986. On the mean particle size and water content of polar mesospheric clouds. Planetary and Space Science 33, 1209–1224.
Thomas, G.E., Olivero, J.J., 1989. Climatology of polar mesospheric clouds, 2. Further analysis of solar mesospheric explorer data. Journal of Geophysical Research 94, 14673–14702.
Thomas, G.E., McPeters, R.D., Jensen, E.J., 1989a. Satellite observations of polar mesospheric clouds by the SBUV radiometer: evidence of a solar-cycle dependence. Journal of Geophysical Research 96, 927–939.
Thomas, G.E., Olivero, J.J., Jensen, E.J., Schröder, W., Toon, O.B., 1989b. Relation between increasing methane and the presence of ice at the mesopause. Nature 338, 490–492.
Thomas, G.E., Olivero, J.J., DeLand, M., Shettle, E.P., 2003. Comment on are noctilucent clouds truly a 'miner's canary' for global change? Transactions, American Geophysical Union 84, 352–353.
Tuzzolino, A.J., et al., 2004. Dust Measurements in the Coma of Comet 81P/Wild 2 by the dust flux monitor instrument. Science 304 (5678), 1776–1780.
Tuzzolino, A.J., et al., 2005. Final results from the space dust (SPADUS) instrument flown aboard the earth-orbiting ARGOS spacecraft. Planetary and Space Science 53 (9), 903–923.
von Zahn, U., 2003. Are noctilucent clouds truly a "miner's canary" of global change? EOS Transactions, American Geophysical Union 84 (28) (pp. 261, 168).
von Zahn, U., Berger, U., 2003. Persistent ice cloud in the midsummer upper mesosphere at high latitudes: Three-dimensional modeling and cloud interactions with ambient water vapor. Journal of Geophysical Research 108, 8451, doi:10.1029/2002JD002409.
Walchli, U., Stegman, J., Witt, G., Cho, J.Y.N., Miller, C.A., Kelley, M.C., Swartz, W.E., 1993. First height comparison of noctilucent clouds and simultaneous PMSE. Geophysical Research Letters 20 (24), 2845–2848.